

**Photoconductive response correction for detectors of terahertz radiation**E. Castro-Camús,<sup>1</sup> L. Fu,<sup>2</sup> J. Lloyd-Hughes,<sup>1</sup> H. H. Tan,<sup>2</sup> C. Jagadish,<sup>2</sup> and M. B. Johnston<sup>1,a)</sup><sup>1</sup>Clarendon Laboratory, Department of Physics, University of Oxford, Parks Road, Oxford OX1 3PU, United Kingdom<sup>2</sup>Department of Electronic Materials Engineering, Research School of Physical Sciences and Engineering, Institute of Advanced Studies, Australian National University, Canberra ACT 0200, Australia

(Received 29 February 2008; accepted 16 June 2008; published online 8 September 2008)

Photoconductive detectors are convenient devices for detecting pulsed terahertz radiation. We have optimized Fe<sup>+</sup> ion-damaged InP materials for photoconductive detector signal to noise performance using dual-energy doses in the range from  $2.5 \times 10^{12}$  to  $1.0 \times 10^{16}$  cm<sup>-2</sup>. Ion implantation allowed the production of semiconducting materials with free-carrier lifetimes between 0.5 and 2.1 ps, which were measured by optical pump terahertz probe spectroscopy. The time resolved photoconductivity of the detector substrates was acquired as a function of time after excitation by 2 nJ pulses from a laser oscillator. These data, when combined with a deconvolution algorithm, provide an excellent spectral response correction to the raw photocurrent signal recorded by the photoconductive detectors. © 2008 American Institute of Physics. [DOI: 10.1063/1.2969035]

**I. INTRODUCTION**

Spectroscopy and imaging with pulsed terahertz radiation are very active fields of science and technology.<sup>1-3</sup> Ultrafast photoconductive terahertz detectors (PCDs) were the first devices used to detect pulsed terahertz radiation<sup>4,5</sup> and now form an integral part of many terahertz time domain spectroscopy (TDS) systems. Auston *et al.*<sup>4</sup> demonstrated the first terahertz PCD in 1984, which followed from Auston's<sup>6</sup> earlier work on picosecond switching of semiconductors. Since then there have been many developments in both PCD design and substrate material science. Design improvements include the development of coplanar strip line,<sup>5</sup> pointed dipole<sup>7</sup> antennas, frequency independent bow-tie antennas,<sup>8</sup> and the incorporation of coupling optics.<sup>5</sup> Recently polarization sensitive PCDs have been developed,<sup>9-11</sup> which are proving useful for terahertz spectroscopy of birefringent and optically active systems.<sup>10</sup> PCDs have been fabricated from many different semiconductor materials including ion-implanted Si-on-sapphire,<sup>4,5</sup> GaAs,<sup>12</sup> InP,<sup>13</sup> and InGaAs,<sup>14</sup> as well as from low-temperature grown GaAs (Ref. 15) and InGaAs.<sup>16</sup> In addition PCD operation has been achieved from devices based on semi-insulating GaAs (Ref. 17) and InP.<sup>18</sup> PCDs have been shown to operate throughout the terahertz band with excellent noise figures and detection bandwidths in excess of 30 THz.<sup>13,15,19</sup>

A PCD measures the electric field of a terahertz pulse as a function of space or time.<sup>5,9,18</sup> In contrast to bolometric detectors, these devices allow all phase and amplitude of the electric field from a terahertz pulse to be recorded.<sup>1</sup> The simplest device design consists of two metal contacts evaporated onto a semiconductor substrate. Typically, these electrodes are connected to the current input of a lock-in amplifier. To operate such a detector, a laser pulse is shone at the gap between the electrodes in order to photogenerate charge car-

riers and hence close the circuit. Once the circuit is closed, an electric field between the electrodes will drive current through the circuit. If a terahertz pulse is focused onto the gap region, its electric field will control the current. How this current relates to the terahertz transient depends on the type of PCD. The two main modes of PCD operation are the (i) direct sampling mode and (ii) integrating mode.

*Direct sampling detectors* are typically fabricated from highly resistive semiconductor substrates that exhibit very short charge-carrier lifetimes. Such materials are usually either grown at low temperature<sup>15,16</sup> or are ion-damaged<sup>4,5,12,13</sup> to create scattering and trapping centers in the crystal structure. In the limiting case, the switch is only closed as long as it is illuminated by the laser pulse. In this case the current in the circuit samples only the point of the terahertz transient that overlaps spatially and temporally with the laser pulse, as shown schematically in Fig. 1(a). Thus the measured photocurrent will be proportional to the strength of the terahertz electric field at that point. By delaying the laser pulse with respect to the terahertz transient by  $\tau$ , it is thus possible to measure the electric field  $E_{\text{terahertz}}$  of the pulse as a function of time  $t$ . Thus the photocurrent is

$$I(\tau) \propto E_{\text{terahertz}}(t = \tau), \quad (1)$$

under the assumption that the laser pulse generates a spike in conductivity in the semiconductor substrate that is of much shorter duration than any feature in the terahertz waveform (typically  $\ll 1$  ps).

*Integrating detectors* are made from materials that have charge-carrier lifetimes that are much longer than the duration of the terahertz transient. The detection method is similar to that for the direct detectors; however, the longer charge-carrier lifetime means that after the PCD is photoexcited the circuit is closed for a period much longer than the duration of the terahertz transient. Therefore, the measured current is proportional to the integral of the electric field of the terahertz transient. As shown schematically in Fig. 1(b),

<sup>a)</sup>Electronic mail: m.johnston@physics.ox.ac.uk.

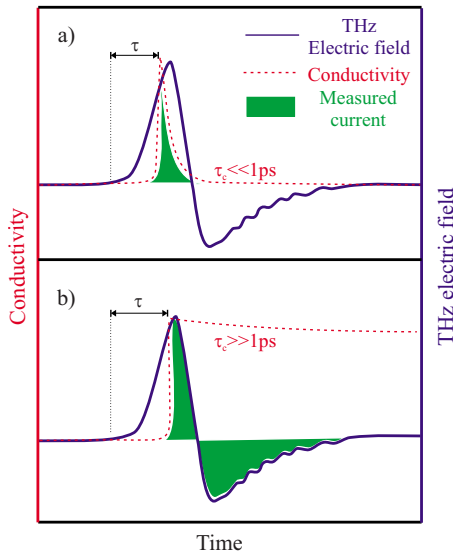


FIG. 1. (Color online) Schematic representation showing a terahertz pulse, the conductivity in a photoconductive receiver, and the current induced between the contacts, which is proportional to the integral of the product of the electric field and the conductivity. In the top and bottom panels, the cases of short ( $\ll 1$  ps) and long ( $\gg 1$  ps) carrier lifetimes in the semiconductor are illustrated.

the lower limit of the integral is the time  $\tau$  in the terahertz transient when the laser pulse overlaps with it. Thus by delaying the laser pulse with respect to the terahertz transient by  $\tau$ , the terahertz electric field  $E_{\text{terahertz}}$  can be recovered from the  $I(\tau)$  data by differentiation with respect to  $\tau$ .<sup>17</sup> That is,

$$I(\tau) \propto \int_{\tau}^{\infty} E_{\text{terahertz}}(t) dt, \quad (2)$$

where it is assumed that the conductivity of the semiconductor rises like a step function upon photoexcitation.

It is a common misconception that high-bandwidth detectors need to be fabricated from short-lifetime materials. As can be seen from Eq. (2), this statement is not correct. The only bandwidth limitation in devices with long photo-carrier lifetimes is that the *rise* time in the photoconductivity must be short, which is a feature usually limited by the duration of the laser pulse rather than by properties of the material. In fact, the reason for using a material with short photogenerated charge-carrier lifetimes is to improve the signal-to-noise ratio (SNR) of the detector rather than to increase the detection bandwidth. Therefore, if noise issues were unimportant, materials such as semi-insulating GaAs, which have nanosecond carrier lifetimes, could be used as substrates for PCDs.

In this study we have optimized materials for PCD applications. In particular we have maximized the SNR of the detectors by adjusting the electrical properties of their substrate materials using ion implantation and subsequent annealing. We have also developed a method that corrects for the spectral response of the optimized devices when the detector falls between the direct sampling and integrating re-

gimes. Both our optimization and spectral response methods relied on data acquired using the technique of optical pump terahertz probe spectroscopy (OPTPS).

## II. OPTICAL PUMP TERAHERTZ PROBE SPECTROSCOPY

OPTPS is a powerful noncontact technique for measuring the optical and electrical properties of bulk<sup>20–22</sup> and nanostructured<sup>23–25</sup> materials. In this method a sample is photoexcited with a femtosecond laser pulse, and the terahertz TDS spectra are measured at short time intervals after the photoexcitation. By comparing the time-gated photoexcited spectra with the “dark” reference spectra the time resolved photoconductivity spectrum is obtained. This technique is much less widely used than terahertz TDS but has proved invaluable for studying ultrafast charge dynamics.<sup>2,26,27</sup>

Most OPTPS studies have been conducted using laser amplifiers to excite samples.<sup>2</sup> This is because the perturbation in the conductivity of a sample photoexcited by high-energy (1  $\mu\text{J}$ –1 mJ) amplified pulses is significantly larger, and hence easier to measure, than that induced by pulses from a laser oscillator (typically  $\leq 10$  nJ). Unfortunately, the charge dynamics in semiconductors excited at high fluence are highly nonlinear and are therefore quite different from those in a device that is photoexcited by pulses from a laser oscillator.<sup>28</sup>

In order to measure the conductivity response of materials for PCDs, it is important to perform OPTPS under conditions as close as possible to those that they operate under. As most terahertz TDS systems rely on laser oscillators to gate their detectors, we decided to use a laser oscillator in our OPTPS measurements.

The OPTPS system that was used in this study is represented in Fig. 2. A chirped mirror laser oscillator (Femtolasers GmbH) was used to generate 10 fs duration laser pulses with an energy of 5 nJ at a repetition rate of 75 MHz (average power 375 mW) and center wavelength of 790 nm. Each laser pulse was split into three parts using dielectric beam splitters. Approximately 2 nJ was used to photoexcite the sample. Another  $\sim 2$  nJ fraction was used to generate a single-cycle terahertz transient by photoexciting a 400  $\mu\text{m}$  gap semi-insulating-GaAs photoconductive emitter that was biased with a square wave of  $\pm 120$  V amplitude and 20 kHz frequency. The remaining fraction of each pulse (0.4 nJ) was used for electro-optic detection of the terahertz waveform in a 200  $\mu\text{m}$  thick (110) ZnTe crystal.

## III. MATERIALS DEVELOPMENT

When high-energy ions are implanted into semiconductors, they generate defects such as vacancies, substituted atoms, interstitial atoms, and dislocations. These defects act both as scattering centers and trapping sites, thereby reducing the mobility and photocarrier lifetime of ion-implanted materials. However, annealing a semiconductor after ion implantation allows the mobility to recover while retaining a significant density of traps, thereby retaining a relatively short photocarrier lifetime. By choosing a combination of

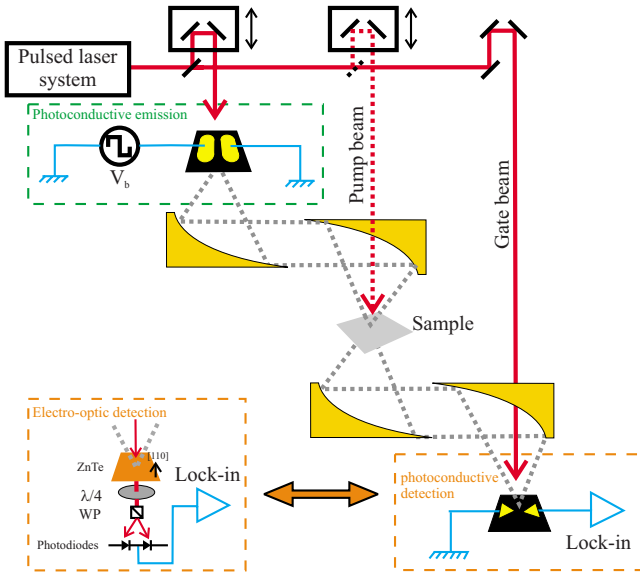


FIG. 2. (Color online) Schematic diagram of the OPTPS system used to measure time resolved photoconductivity. Here  $V_b$  is the bias voltage of a square wave source that was applied across a photoconductive emitter.  $\lambda/4$  and WP label a quarter wave plate and Wollaston prism, respectively. The same apparatus was converted to a standard terahertz TDS system by blocking the “pump beam” and replacing the electro-optic detection components with a PCD.

appropriate implantation dose and energy in addition to correct annealing temperature, the electronics properties of a semiconductor can be controlled precisely.<sup>29,30</sup>

For this study the tandem accelerator at the Australian National University<sup>31</sup> was used to implant semi-insulating InP samples with  $\text{Fe}^+$  ions. Each sample was implanted with a combination of 2.0 and 0.8 MeV ions. The vacancy concentration was first modeled using the *stopping and range of ions in matter* (SRIM) software<sup>32</sup> in order to generate an almost constant damage profile over the absorption depth for near-infrared photons ( $\sim 1 \mu\text{m}$ ). For example, the calculated vacancy density for a chosen dose of  $1 \times 10^{16}$  and  $2.5 \times 10^{15} \text{ cm}^{-2}$  at 2.0 and 0.8 MeV, respectively, is shown in the inset of Fig. 3. All samples were subsequently annealed at  $500^\circ\text{C}$  for 30 min in a  $\text{PH}_3$  atmosphere. The implantation conditions for the four samples used in this study are listed in Table I.

#### IV. MATERIALS CHARACTERIZATION

The time resolved photoconductivity  $\sigma(t)$  of the samples listed in Table I was measured using our OPTPS system.<sup>33</sup> The samples were photoexcited by 2 nJ laser pulses imaged to a  $\sim 1 \text{ mm}$  full-width-at-half-maximum (FWHM) spot. Terahertz radiation was focused on the sample to a near diffraction limited spot (FWHM waist  $\sim 300 \mu\text{m}$  at 1 THz). Thus the terahertz radiation probes conductivity over an area of relatively uniform photon fluence  $\sim 2.5 \times 10^{11} \text{ cm}^{-2}$ . This excitation density was chosen as it is typical of the densities used in most terahertz TDS and imaging systems reported to date. Furthermore, for this combination of fluence and ion-implantation doses, the variation in the optical absorption coefficient is expected to be negligible and therefore to fall in the linear regime.<sup>34</sup> The time resolved terahertz conduc-

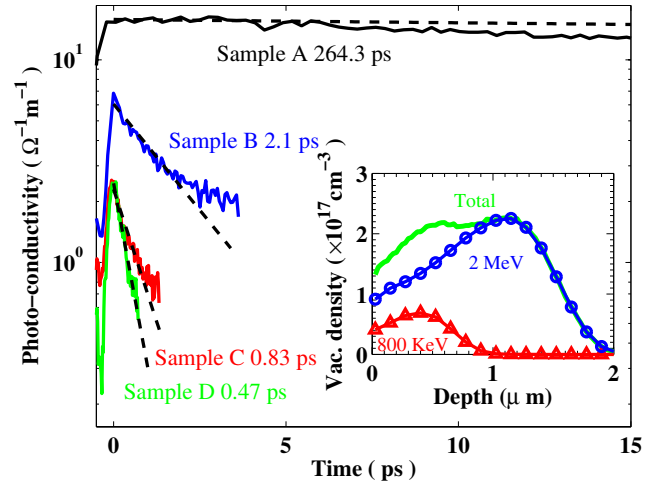


FIG. 3. (Color online) Conductivity of Fe ion-implanted InP measured using OPTPS at various implantation doses. The dotted curves are exponential decays fitted to the experimental data. Inset: simulated vacancy concentration [using SRIM software (Ref. 32)] for InP implanted with  $\text{Fe}^+$  ions at doses  $1 \times 10^{13}$  and  $2.5 \times 10^{12} \text{ cm}^{-2}$  at 2.0 and 0.8 MeV, respectively, considering 99.9% of instantaneous vacancy anneal at implantation (room) temperature; each dose generates a density of vacancies shown in circles (0.8 MeV) and triangles (2 MeV); the total vacancy profile is the sum of both contributions (continuous line).

tivity data from the four samples are shown in Fig. 3. These conductivity data are independent of any particular model of carrier dynamics in the bulk material and provide all the information necessary to correct the spectral response of PCDs fabricated from the measured materials. However for our analysis of device performance, it is informative to extract simple parameters that do rely on modeling. As shown by the dashed lines in Fig. 3, the initial decay of  $\sigma(t)$  was monoexponential for all ion doses and can be fitted as

$$\sigma(t) = \sigma_0 e^{-t/\tau_c}, \quad (3)$$

where  $\sigma_0$  is the peak photoconductivity of the sample and  $\tau_c$  is the photoconductivity lifetime. These parameters were extracted directly from the data presented in Fig. 3 by performing a least-squares exponential fit to the initial part of the decay curves (Table II).

In order to separate the mobility  $\mu$  and charge density  $n$  from the raw conductivity data  $\sigma(t) = e\mu(t)n(t)$ , we assumed that the mobility was time-independent  $\mu(t) = \mu_0$ . This is a reasonable assumption for Drude-type semiconductors excited by photons with energies just above their band edge at the excitation densities used in this study.<sup>29,35</sup> Furthermore it

TABLE I. Doses of  $\text{Fe}^+$  ions implanted into semi-insulating InP substrates for each of the samples (A–D) used in this study. Ions were accelerated to two different energies, 0.8 and 2.0 MeV, to improve the uniformity of vacancies as a function of depth into the InP substrate.

Sample	Dose at 2 MeV ( $\text{cm}^{-2}$ )	Dose at 0.8 eV ( $\text{cm}^{-2}$ )
A	0	0
B	$1 \times 10^{13}$	$2.5 \times 10^{12}$
C	$5 \times 10^{14}$	$1.25 \times 10^{14}$
D	$1 \times 10^{16}$	$2.5 \times 10^{15}$

TABLE II. The peak photoinduced conductivity  $\sigma_0$ , conductivity lifetime  $\tau_c$ , and mobility  $\mu_0$  of the Fe<sup>+</sup> ion-implanted semi-insulating InP samples described in Table I. These parameters were extracted from the OPTPS data presented in Fig. 3.

Sample	$\sigma_0$ ( $\Omega^{-1} \text{ cm}^{-1}$ )	$\tau_c$ (ps)	$\mu_0$ ( $\mu_{\text{InP}}$ )
A	$0.158 \pm 0.005$	$264.3 \pm 48$	$1.00 \pm 0.05$
B	$0.066 \pm 0.006$	$2.1 \pm 0.3$	$0.42 \pm 0.04$
C	$0.026 \pm 0.0005$	$0.8 \pm 0.1$	$0.16 \pm 0.01$
D	$0.025 \pm 0.0005$	$0.5 \pm 0.1$	$0.15 \pm 0.01$

has been shown that trapping of charge carriers at impurities is the most important mechanism for reducing  $n$  after pulsed photoexcitation.<sup>30</sup> Therefore using our assumptions,  $\tau_c$  is also the characteristic trapping time for photocarriers. Thus the effective electron mobility  $\mu_0$  was calculated from the extracted value of  $\sigma_0$  and the initial photocarrier density. The extracted values for all these parameters are listed in Table II.

In Fig. 3, it is clear that as the ion dose is increased, the lifetime of the photoconductivity drops, but unfortunately this is at the expense of a drop in the peak conductivity. Sample B showed a good compromise between having a short photoconductivity lifetime while maintaining a relatively high peak photoconductivity. However, it can be seen that the photoconductivity lifetime of sample B is  $2.1 \pm 0.3$  ps, which falls between the limits required for either a “direct sampling” or an “integrating” PCD material. Thus in a terahertz TDS system, the photocurrent measured from a device fabricated from sample B would not be proportional to the terahertz electric field or its integral.

## V. DEVICE CHARACTERIZATION

Terahertz PCDs were fabricated from samples A, B, C, and D. A bow-tie electrode geometry was chosen owing to its relatively flat frequency response across the terahertz band.<sup>36</sup> The devices were mounted on the OPTPS system described previously. However for these experiments, the “pump” laser beam was blocked, and the detection system was replaced by bow-tie detectors (as shown in Fig. 2). Thus the system mimicked a standard terahertz TDS system. The 0.4 nJ laser pulses (focused on a  $\sim 100$   $\mu\text{m}$  spot) were used to gate the photoconductive receiver. The current between the terminals of the photoconductive switch was recorded using a lock-in amplifier with a time constant of 100 ms locked to the 20 kHz square wave that biased the terahertz emitter.

The raw photocurrent signal from the devices is shown in Fig. 4(a). Since the terahertz scans were recorded under identical conditions for all three devices, it is possible to compare their relative responsivities directly. It can be seen that a PCD fabricated from the sample with the lowest implantation dose gives the largest current response to the terahertz transient, with the responsivity degrading with increased ion dose. It was not possible to obtain a photocurrent signal from the device fabricated on the unimplanted control sample (A) owing to high noise levels.

It is informative to compare the response of the PCDs with the material properties obtained from OPTPS. There is a

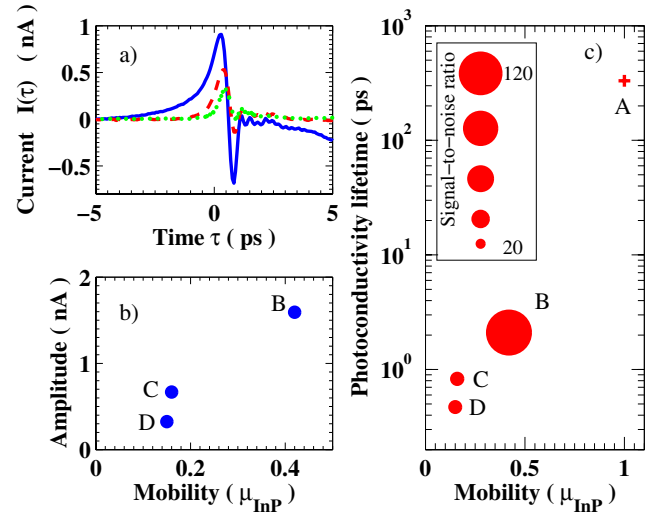


FIG. 4. (Color online) (a) Raw photocurrent through bow-tie PCDs fabricated from the InP: Fe<sup>+</sup> materials: B (solid line), C (dashed line), and D (dots) described in Table I. The data are shown as a function of the time difference  $\tau$  between the arrival of a terahertz transient and a gating laser pulse at the gap region of the PCD. (b) The relationship between the amplitude of the signal shown in (a) and the mobility of the InP:Fe<sup>+</sup> material from which the PCDs were fabricated. (c) Representation of the relationship between the materials properties (photocarrier lifetime and mobility) of the PCD substrate and the SNR of the PCD.

linear relation between the responsivity of a device and the mobility of its substrate as illustrated in Fig. 4(b). This result is consistent with the linear relation between photocurrent and mobility predicted by Eqs. (6) and (7), which are presented in Sec. VI.

The primary sources of noise in a photoconductive receiver are Johnson–Nyquist<sup>37,38</sup> and laser shot noise.<sup>18</sup> Laser shot noise is independent of the particular material or device; therefore, here it is only important to consider Johnson–Nyquist noise.<sup>10</sup> The Johnson–Nyquist noise current  $I_{J-N}$  is caused by thermal fluctuations of the charge carriers in a material and may be expressed as

$$I_{J-N} = \sqrt{\frac{4k_B T \Delta f}{\langle R \rangle}}, \quad (4)$$

where  $k_B$  is Boltzmann’s constant,  $\Delta f$  is the measurement bandwidth, and  $\langle R \rangle$  is the time average resistance of the device operating at a temperature  $T$ . It is important to note that the noise current is inversely proportional to the square root of the *average* resistance of the device. Therefore, shorter lifetime materials, which have a much larger average resistivity when illuminated with femtosecond laser pulses, should produce devices with a lower noise current.

An ideal PCD device would have a high current responsivity and a low current noise. For ion-implanted materials the current noise drops with increasing dose, but this is at the expense of current responsivity. Thus it is important to optimize materials in order to maximize device SNRs.

The SNR was calculated for each device (by the method described in Ref. 10) and is plotted on a graph of material parameters in Fig. 4(c). An ideal material from which to fabricate a PCD should have parameters corresponding to the bottom right-hand corner of Fig. 4(c). This is because the



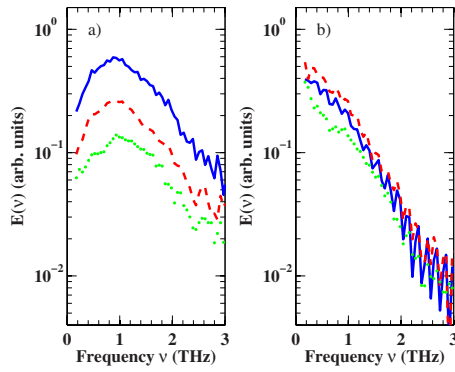


FIG. 5. (Color online) Comparison of terahertz spectra calculated by (a) differentiation and (b) deconvolution of the photocurrent data shown in Fig. 4(a). The processed data are from PCDs fabricated on InP:Fe<sup>+</sup> substrates B (solid line), C (dashed line), and D (dots), as described in Table I. The spectra calculated by differentiation show strong dependence on the ion dose while the deconvolved spectra show very similar curves for the three ion implantation doses.

responsivity of a device is proportional to the mobility of its substrate and its noise current is predicted to drop with photoconductive lifetime. The measured values of SNR for the devices (represented by the circle-radius on the figure) agree with this analysis. Clearly the device fabricated from sample B shows by far the best performance owing to its high responsivity and reasonable noise current. Such parameter space maps are useful for optimizing materials without the time-consuming process of fabricating and testing devices in a terahertz TDS system.

## VI. SEMICONDUCTOR RESPONSE AND DECONVOLUTION

It is interesting, if not somewhat unfortunate, that the materials which produce PCDs with the highest SNRs have photoconductive lifetimes similar to the duration of a terahertz transient. Thus the raw  $I(\tau)$  output from these high-performance devices cannot be immediately translated into terahertz electric field data [ $E_{\text{terahertz}}(t)$ ] by either a proportionality constant or by differentiation. In this section we demonstrate that the time resolved conductivity of a substrate material is all the data that is required to correct for the response of any PCD fabricated from that substrate.

As an illustration of this problem, the Fourier transforms of the derivative of the raw photocurrent data in Fig. 4(a) are presented in Fig. 5(a). These differentiated data would be proportional to the terahertz electric field if the device could be classified as an “integrating” PCD. As the terahertz source was identical when measuring each of the device, if correctly reproduced, the terahertz spectra shown in Fig. 5(a) should have been identical to each other. There is clearly a large discrepancy between the spectral response of these devices. However, using the raw OPTPS data, we are able to correct for the spectral response of each detector as shown in Fig. 5(b). The spectral response method that we have developed is described below.

The current induced between the two contacts of the photoconductive receiver may be expressed as<sup>18,19,39</sup>

$$I(\tau) \propto \int_{-\infty}^{+\infty} E_{\text{terahertz}}(t) \sigma(t - \tau) dt, \quad (5)$$

where  $E_{\text{terahertz}}(t)$  is the effective<sup>40</sup> electric field of the terahertz transient at the PCD and  $\sigma(\tau)$  is the time resolved conductivity of the device substrate. Since a single OPTPS measurement of a substrate material provides a direct measurement of  $\sigma(\tau)$ , it is then possible to extract the form of the terahertz transient  $E_{\text{terahertz}}(t)$  numerically for each photocurrent data set  $I(\tau)$  measured by any PCD fabricated from that material.

Although Eq. (5) contains all the information required to correct the spectral response of a PCD, it is useful to develop an approximate but fast deconvolution method. As shown in the Appendix, Eq. (5) may be written as

$$I(\tau) = \beta \int_{-\infty}^{+\infty} E_{\text{terahertz}}(t) \Phi(t - \tau) dt, \quad (6)$$

where

$$\beta = \frac{\mu_0 e P_G T_{12} \lambda}{hc \Sigma}, \quad (7)$$

$\Phi(t)$  is the normalized time dependent conductivity,  $T_{12}$  is the Fresnel transmission coefficient for light from a laser gate beam of center wavelength  $\lambda$ , waist of standard deviation  $\Sigma$ , and average power  $P_G$  entering the PCD from a vacuum. Here  $e$ ,  $h$ , and  $c$  are the electronic charge, Planck’s constant, and the speed of light in a vacuum, respectively.

The physics of both the photogeneration and trapping of carriers are contained in  $\Phi$ . In the simplest approximation, a  $\delta$ -function-like laser pulse and infinite trapping and recombination lifetimes can be assumed. In this case  $\Phi$  is a step function and the electric field can be recovered simply by differentiating both sides of this equation.

In reality  $\Phi$  has a more complicated shape so a more sophisticated approach is required. Equation (6) is a Fredholm integral equation of the first kind that can be seen as a convolution, in the Fourier sense,<sup>41</sup> of functions  $E$  and  $\Phi$ . Its solution is given by

$$E_{\text{terahertz}}(t) = \beta \mathcal{F}^{-1} \left[ \frac{\mathcal{F}(I)}{\mathcal{F}(\Phi)} \right], \quad (8)$$

where  $\mathcal{F}$  is the Fourier transform operator.

Since in most terahertz TDS systems the duration of the laser pulse is much shorter than the terahertz transient to be measured ( $t_0 \ll 1$  ps), it is possible to approximate  $\Phi(t)$  as

$$\Phi(t) \approx H(t) e^{-t/\tau_c}, \quad (9)$$

where  $H$  is the unit step function. This approximation avoids the need to numerically invert Eq. (8); thus, the effective terahertz electric field may be expressed in the simple analytic form

$$E_{\text{terahertz}}(t) = \beta \mathcal{F}^{-1} \left[ \mathcal{F}(I) \left( \frac{1}{\tau_c} + i\omega \right) \right]. \quad (10)$$

This equation was used to deconvolve the terahertz signal  $E_{\text{terahertz}}(t)$  from the photocurrent data  $I(\tau)$  presented in Fig. 4. The deconvolved data from the three PCDs with

widely varying material properties are shown in Fig. 5(b). The data sets overlap, illustrating the success of using the OPTPS data to produce an accurate correction for the electronic response of a PCS. For comparison the spectra obtained from a simple differentiation shown in Fig. 5(a) are strongly dependent on which detector was used. In addition, the corrected spectra shown in Fig. 5(b) give a good indication of the true spectrum<sup>40</sup> emitted from the photoconductive switch used in our experiments since the transfer function for a bow-tie antenna has only a weak frequency dependence<sup>8</sup> and since large (3 in.) reflective optics<sup>30</sup> were used to focus the terahertz pulses.

## VII. CONCLUSION

We have used OPTPS to obtain time resolved data on the photoinduced conductivity of ion-implanted InP. The ideal materials for PCD applications have a short photogenerated charge-carrier lifetime to minimize their noise current and a high peak photoconductivity to maximize its responsivity. When optimizing a material, a balance must be obtained between these two constraints. Apart from allowing materials to be optimized before device fabrication, the time resolved photoconductivity data also provide all the information required to correct for the spectral response of PCDs. Using a deconvolution method, we have corrected the spectral response of a range of PCDs. The methods presented are not limited to InP materials and may be used to correct the spectral response of PCDs fabricated on any material. Thus from a single measurement of the time resolved conductivity of a semiconductor, we have shown that it is possible to generate a fast and convenient spectral response correction that can be applied to any data set acquired from any PCD fabricated from that semiconductor.

The authors would like to thank the EPSRC (UK) and the Australian Research Council for supporting this work.

## APPENDIX: DERIVATION OF PCD RESPONSE

The current generated between the two contacts of a PCD is given by

$$I(\tau) = R \int_{-\infty}^{+\infty} \iint_{\Pi} \mathbf{J}(\mathbf{r}, t, \tau) \cdot d\mathbf{s} dt, \quad (\text{A1})$$

where  $\Pi$  is a surface separating the two contacts,  $R$  is the laser's repetition rate, and  $\mathbf{J}(\mathbf{r}, t, \tau)$  is the current density generated by one laser pulse and one terahertz transient with relative delay  $\tau$ .  $\mathbf{J}$  depends on the conductivity of the substrate and the electric field at each point

$$\mathbf{J}(\mathbf{r}, t, \tau) = \mu_0 e n(\mathbf{r}, t - \tau) \mathbf{E}_{\text{terahertz}}(\mathbf{r}, t), \quad (\text{A2})$$

where,  $\mu_0$  is the semiconductor's mobility,  $e$  is the electron charge,  $n(\mathbf{r}, t)$  is the charge carrier density, and  $\mathbf{E}_{\text{terahertz}}(\mathbf{r}, t)$  is the effective terahertz electric field incident on the PCD. Assuming that  $\mathbf{E}_{\text{terahertz}}$  is spatially constant over the active region of the photoconductive detector and also that the gating laser beam has a Gaussian spatial profile with standard deviation  $\Sigma$ , the time domain shape of the terahertz single

cycle in the direction of the unit vector  $\hat{\mathbf{u}}$  parallel to  $d\mathbf{s}$  will be given by

$$E(t) = \mathbf{E}_{\text{terahertz}}(0, t) \cdot \hat{\mathbf{u}} \quad (\text{A3})$$

and  $n(\mathbf{r}, t)$  by

$$n(\mathbf{r}, t) = \frac{P_G T_{12} \lambda}{R h c \Sigma^2 \xi \sqrt{\pi}} \exp \left[ -\frac{x^2 + y^2}{\Sigma^2} - \frac{z}{\xi} \Phi(t) \right], \quad (\text{A4})$$

where  $\Phi(t)$  is the temporal part of the conductivity response of the semiconductor,  $T_{12}$  is the Fresnel transmission coefficient for light from a laser gate beam of center wavelength  $\lambda$ , absorption depth  $\xi$ , and average power  $P_G$  entering the semiconductor substrate of the PCD from a vacuum. Here  $h$  is Planck's constant and  $c$  is the speed of light in a vacuum.

Therefore, the current measured through a PCD may be expressed as

$$I(\tau) = \frac{\mu_0 e P_G T_{12} \lambda}{h c \Sigma} \int_{-\infty}^{+\infty} E(t) \Phi(t - \tau) dt, \quad (\text{A5})$$

since

$$\frac{\mu_0 e P_G T_{12} \lambda}{h c \Sigma^2 \xi \sqrt{\pi}} \iint_{\Pi} \exp \left( -\frac{x^2 + y^2}{\Sigma^2} - \frac{z}{\xi} \right) d\mathbf{s} = \frac{\mu_0 e P_G T_{12} \lambda}{h c \Sigma}. \quad (\text{A6})$$

- <sup>1</sup>W. L. Chan, J. Deibel, and D. M. Mittleman, *Rep. Prog. Phys.* **70**, 1325 (2007).
- <sup>2</sup>C. A. Schmuttenmaer, *Chem. Rev. (Washington, D.C.)* **104**, 1759 (2004).
- <sup>3</sup>M. Tonouchi, *Nat. Photonics* **1**, 97 (2007).
- <sup>4</sup>D. H. Auston, K. P. Cheung, and P. R. Smith, *Appl. Phys. Lett.* **45**, 284 (1984).
- <sup>5</sup>M. Vanexter, C. Fattering, and D. Grischkowsky, *Appl. Phys. Lett.* **55**, 337 (1989).
- <sup>6</sup>D. H. Auston, *Appl. Phys. Lett.* **26**, 101 (1975).
- <sup>7</sup>Y. Cai, I. Brener, J. Lopata, J. Wynn, L. Pfeiffer, and J. Federici, *Appl. Phys. Lett.* **71**, 2076 (1997).
- <sup>8</sup>R. Yano, H. Gotoh, Y. Hirayama, S. Miyashita, Y. Kadoya, and T. Hattori, *J. Appl. Phys.* **97**, 103103 (2005).
- <sup>9</sup>E. Castro-Camus, J. Lloyd-Hughes, M. B. Johnston, M. D. Fraser, H. H. Tan, and C. Jagadish, *Appl. Phys. Lett.* **86**, 254102 (2005).
- <sup>10</sup>E. Castro-Camus, J. Lloyd-Hughes, L. Fu, H. H. Tan, C. Jagadish, and M. B. Johnston, *Opt. Express* **15**, 7047 (2007).
- <sup>11</sup>H. Makabe, Y. Hirota, M. Tani, and M. Hangyo, *Opt. Express* **15**, 11650 (2007).
- <sup>12</sup>T. A. Liu, M. Tani, M. Nakajima, M. Hangyo, and C. L. Pan, *Appl. Phys. Lett.* **83**, 1322 (2003).
- <sup>13</sup>T. A. Liu, M. Tani, M. Nakajima, M. Hangyo, K. Sakai, S. Nakashima, and C. L. Pan, *Opt. Express* **12**, 2954 (2004).
- <sup>14</sup>M. Suzuki and M. Tonouchi, *Appl. Phys. Lett.* **86**, 163504 (2005).
- <sup>15</sup>S. Kono, M. Tani, P. Gu, and K. Sakai, *Appl. Phys. Lett.* **77**, 4104 (2000).
- <sup>16</sup>A. Takazato, M. Kamakura, T. Matsui, J. Kitagawa, and Y. Kadoya, *Appl. Phys. Lett.* **90**, 101119 (2007).
- <sup>17</sup>F. G. Sun, G. A. Wagoner, and X. C. Zhang, *Appl. Phys. Lett.* **67**, 1656 (1995).
- <sup>18</sup>M. Tani, K. Sakai, and H. Mimura, *Jpn. J. Appl. Phys., Part 2* **36**, L1175 (1997).
- <sup>19</sup>S. Kono, M. Tani, and K. Sakai, *Appl. Phys. Lett.* **79**, 898 (2001).
- <sup>20</sup>J. Lloyd-Hughes, S. K. E. Merchant, L. Fu, H. H. Tan, C. Jagadish, E. Castro-Camus, and M. B. Johnston, *Appl. Phys. Lett.* **89**, 232102 (2006).
- <sup>21</sup>M. C. Beard, G. M. Turner, and C. A. Schmuttenmaer, *Phys. Rev. B* **62**, 15764 (2000).
- <sup>22</sup>S. S. Prabhu, S. E. Ralph, M. R. Melloch, and E. S. Harmon, *Appl. Phys. Lett.* **70**, 2419 (1997).
- <sup>23</sup>P. Parkinson, J. Lloyd-Hughes, Q. Gao, H. H. Tan, C. Jagadish, M. B. Johnston, and L. M. Herz, *Nano Lett.* **7**, 2162 (2007).
- <sup>24</sup>J. B. Baxter and C. A. Schmuttenmaer, *J. Phys. Chem. B* **110**, 25229

- (2006).
- <sup>25</sup>D. G. Cooke, A. N. MacDonald, A. Hryciw, J. Wang, Q. Li, A. Meldrum, and F. A. Hegmann, *Phys. Rev. B* **73**, 193311 (2006).
- <sup>26</sup>R. Huber, F. Tauser, A. Brodschelm, M. Bichler, G. Abstreiter, and A. Leitenstorfer, *Nature (London)* **414**, 286 (2001).
- <sup>27</sup>R. Huber, C. Kübler, S. Tubel, A. Leitenstorfer, Q. T. Vu, H. Haug, F. Kohler, and M. C. Amann, *Phys. Rev. Lett.* **94**, 027401 (2005).
- <sup>28</sup>J. Shah, *Ultrafast Spectroscopy of Semiconductors and Semiconductor Nanostructures*, 2nd ed. (Springer, Berlin, 1999).
- <sup>29</sup>J. Lloyd-Hughes, E. Castro-Camus, and M. B. Johnston, *Solid State Commun.* **136**, 595 (2005).
- <sup>30</sup>J. Lloyd-Hughes, E. Castro-Camus, M. D. Fraser, C. Jagadish, and M. B. Johnston, *Phys. Rev. B* **70**, 235330 (2004).
- <sup>31</sup>A. Krotkus, S. Marcinkevicius, J. Jasinski, M. Kaminska, H. H. Tan, and C. Jagadish, *Appl. Phys. Lett.* **66**, 3304 (1995).
- <sup>32</sup>J. F. Ziegler and J. P. Biersack, SRIM, 2003, available online at <http://www.srim.org>.
- <sup>33</sup>OPTPS is capable of measuring the full frequency dependent photo-conductivity  $\sigma(\omega, t)$  of a material. In this work we assume that the conductivity is frequency independent  $\sigma(\omega, t) = \sigma(t)$ , over the range of frequencies that we would like to detect with our PCD ( $\approx 0.1 - 3$  THz). Since this frequency range is well below the plasma frequency of the photoexcited PCS, the assumption is justified.
- <sup>34</sup>M. J. Lederer, B. Luther-Davies, H. H. Tan, C. Jagadish, M. Haiml, U. Siegner, and U. Keller, *Appl. Phys. Lett.* **74**, 1993 (1999).
- <sup>35</sup>M. C. Beard, G. M. Turner, and C. A. Schmuttenmaer, *J. Appl. Phys.* **90**, 5915 (2001).
- <sup>36</sup>M. Tani, S. Matsuura, K. Sakai, and S. Nakashima, *Appl. Opt.* **36**, 7853 (1997).
- <sup>37</sup>J. B. Johnson, *Phys. Rev.* **32**, 97 (1928).
- <sup>38</sup>H. Nyquist, *Phys. Rev.* **32**, 110 (1928).
- <sup>39</sup>S. G. Park, M. R. Melloch, and A. M. Weiner, *Appl. Phys. Lett.* **73**, 3184 (1998).
- <sup>40</sup>It should be noted that to obtain the true form of the free space electric field of the terahertz transient  $\tilde{E}_{\text{THz}}(t)$ , the dielectric properties of the antenna and photo-excited substrate would need to be considered as they are spectrally dependent. That is  $\tilde{E}_{\text{THz}}(\omega) = \gamma(\omega)E_{\text{THz}}(\omega)$ , where  $\gamma(\omega)$  is a response function at terahertz frequencies  $\omega$ .  $\gamma(\omega)$  is dependent on the PCD antenna geometry and the dielectric properties of the device.
- <sup>41</sup>G. Arfken, *Mathematical Methods for Physicists*, 3rd ed. (Academic, New York, 1985).